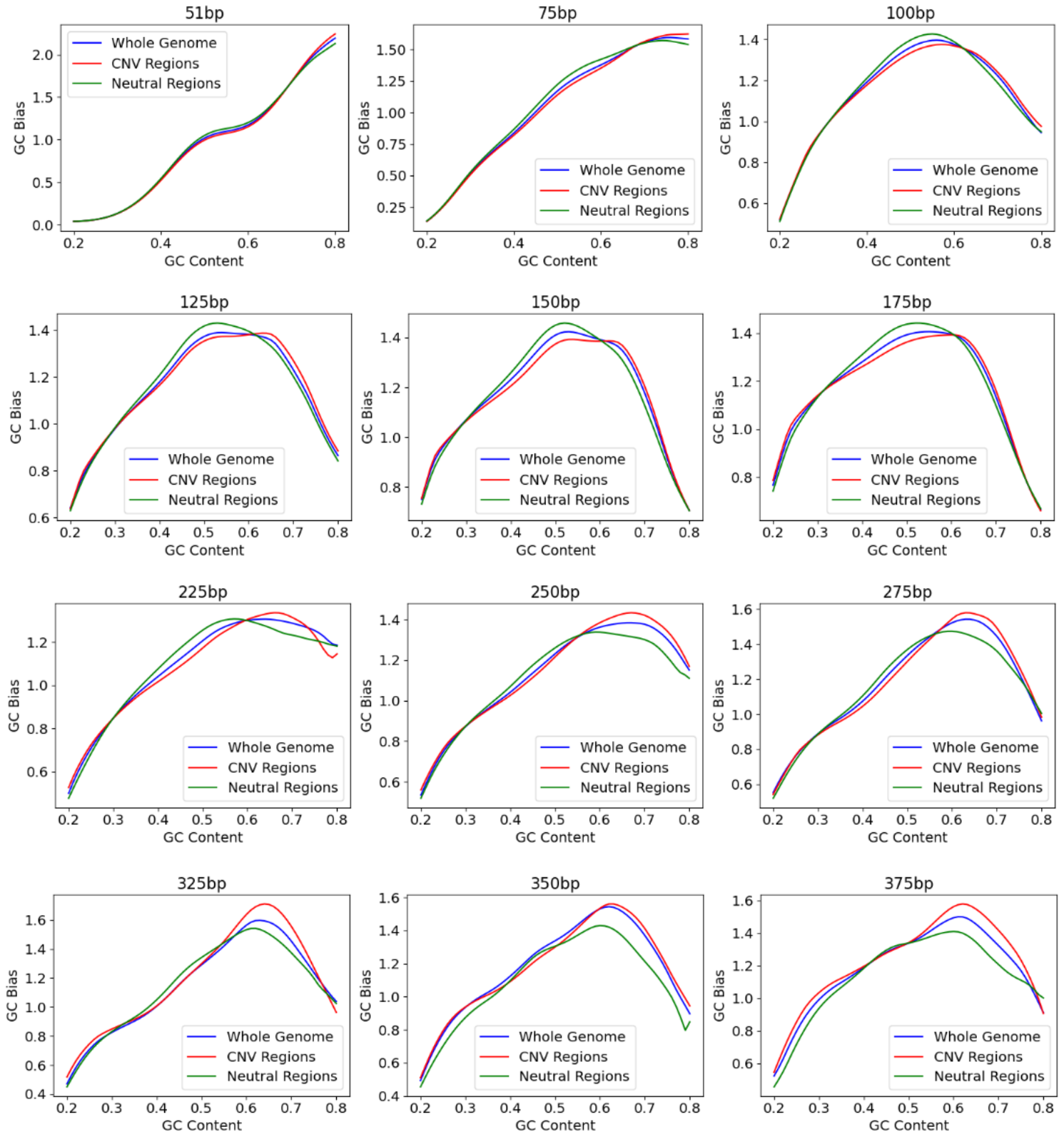
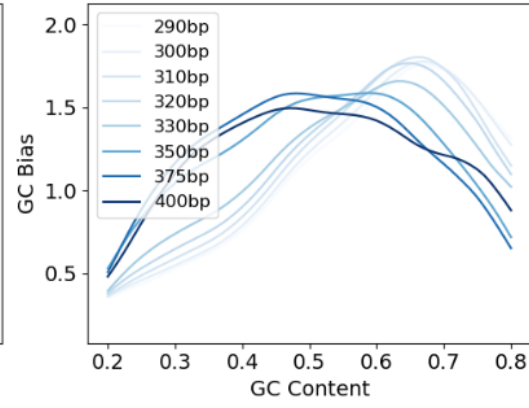
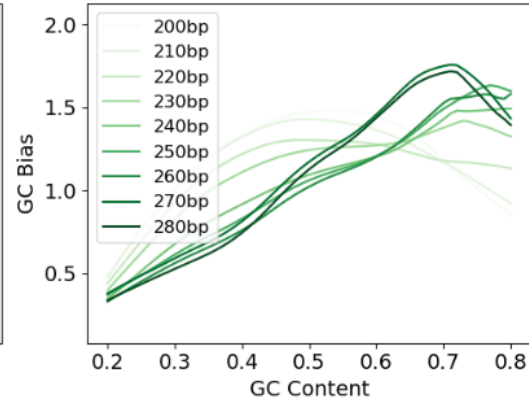
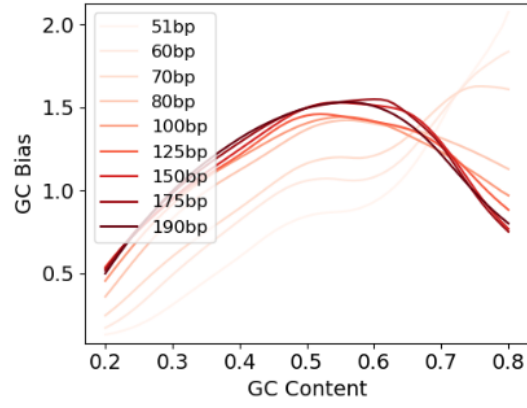


Suppl Fig S1: Base density in reference genome for full fragment GC context vs 10bp clipped (from both ends) fragment GC context for different fragment lengths of a healthy sample

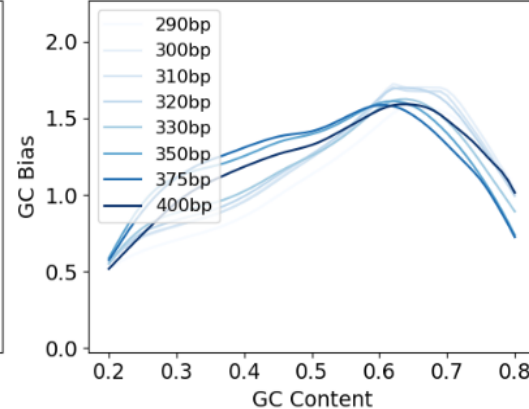
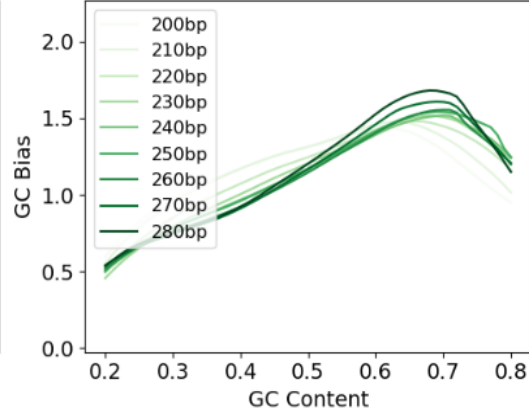
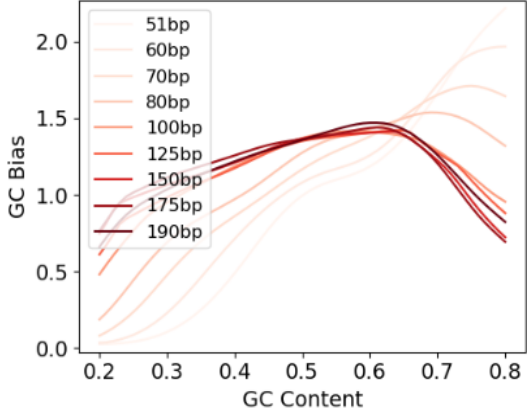


Suppl Fig S2: GC bias curve based on whole genome, neutral and copy number variant (CNV) regions for different fragment lengths of a colon cancer sample

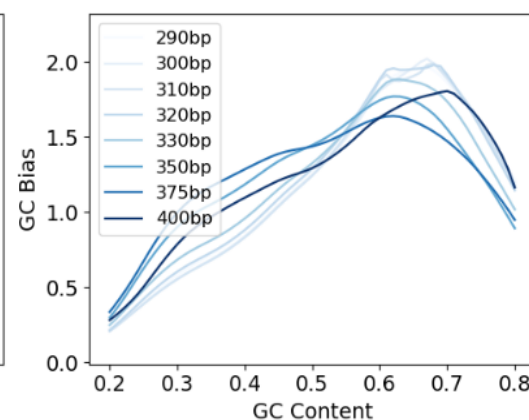
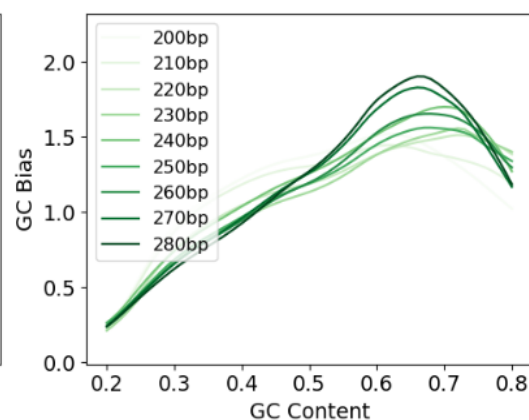
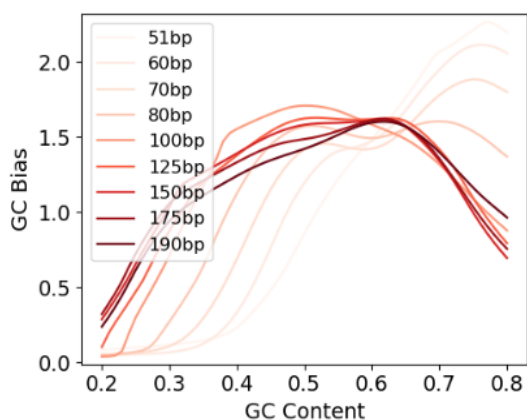
Healthy Sample



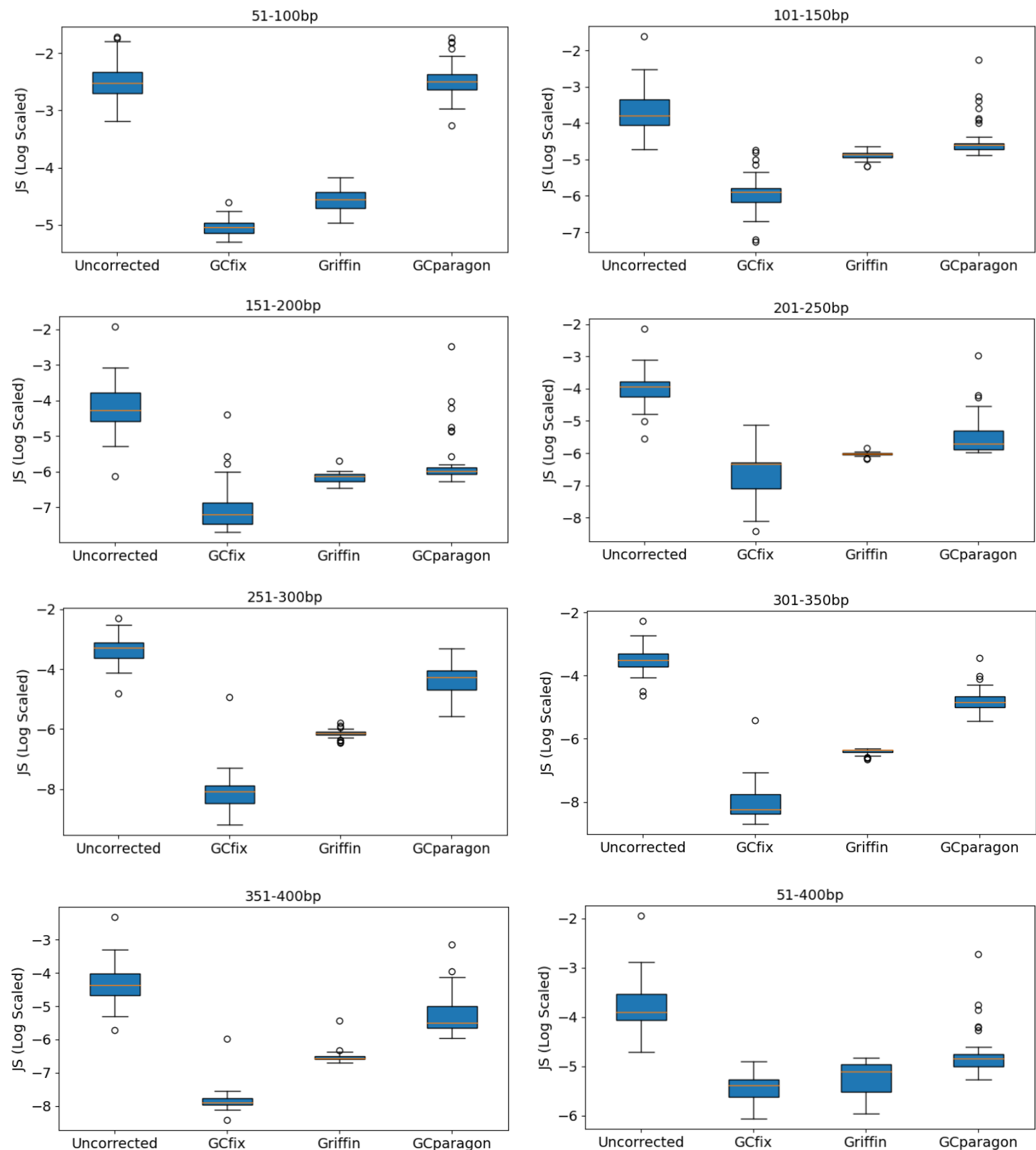
Colon Cancer Sample



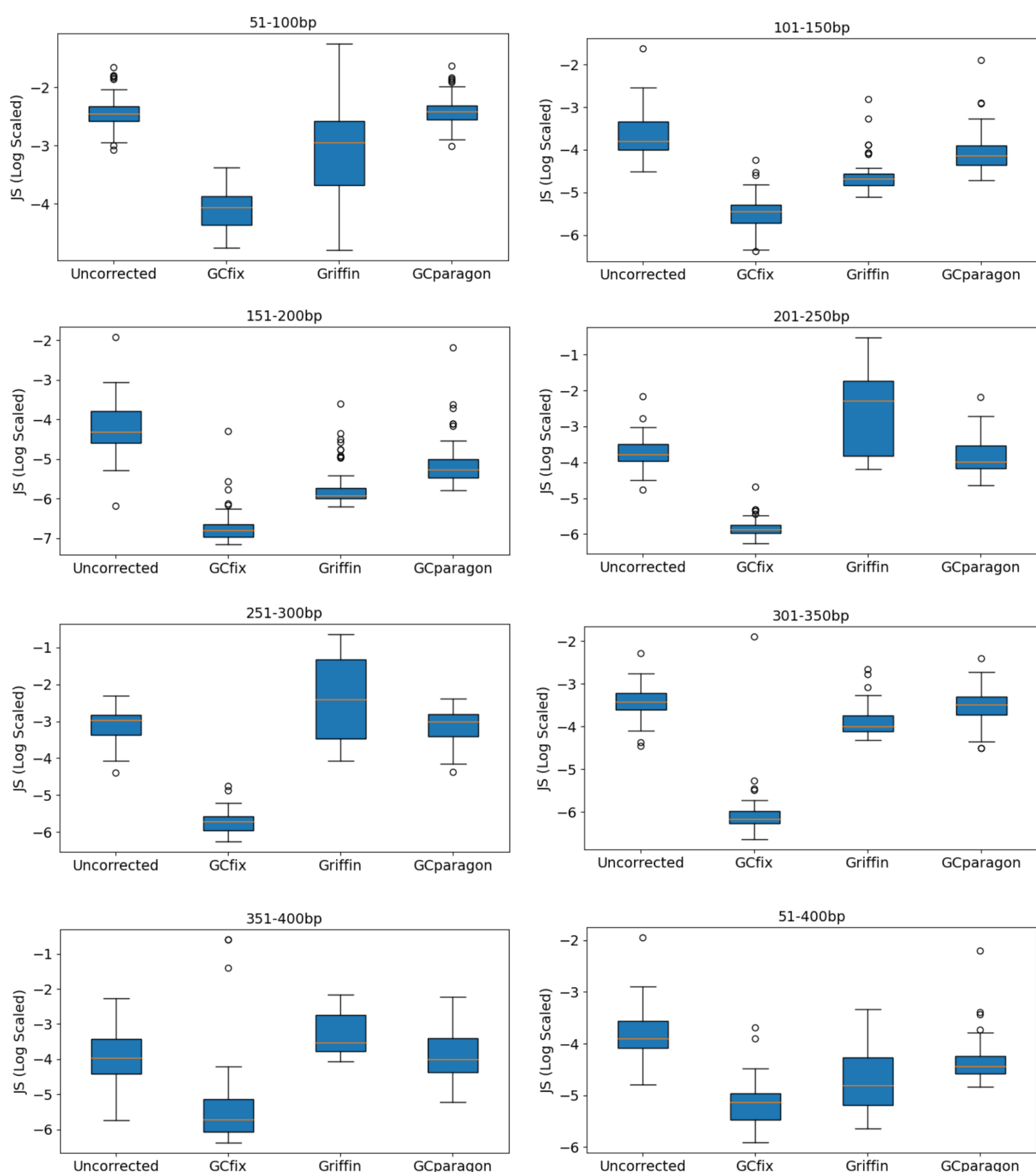
Breast Cancer Sample



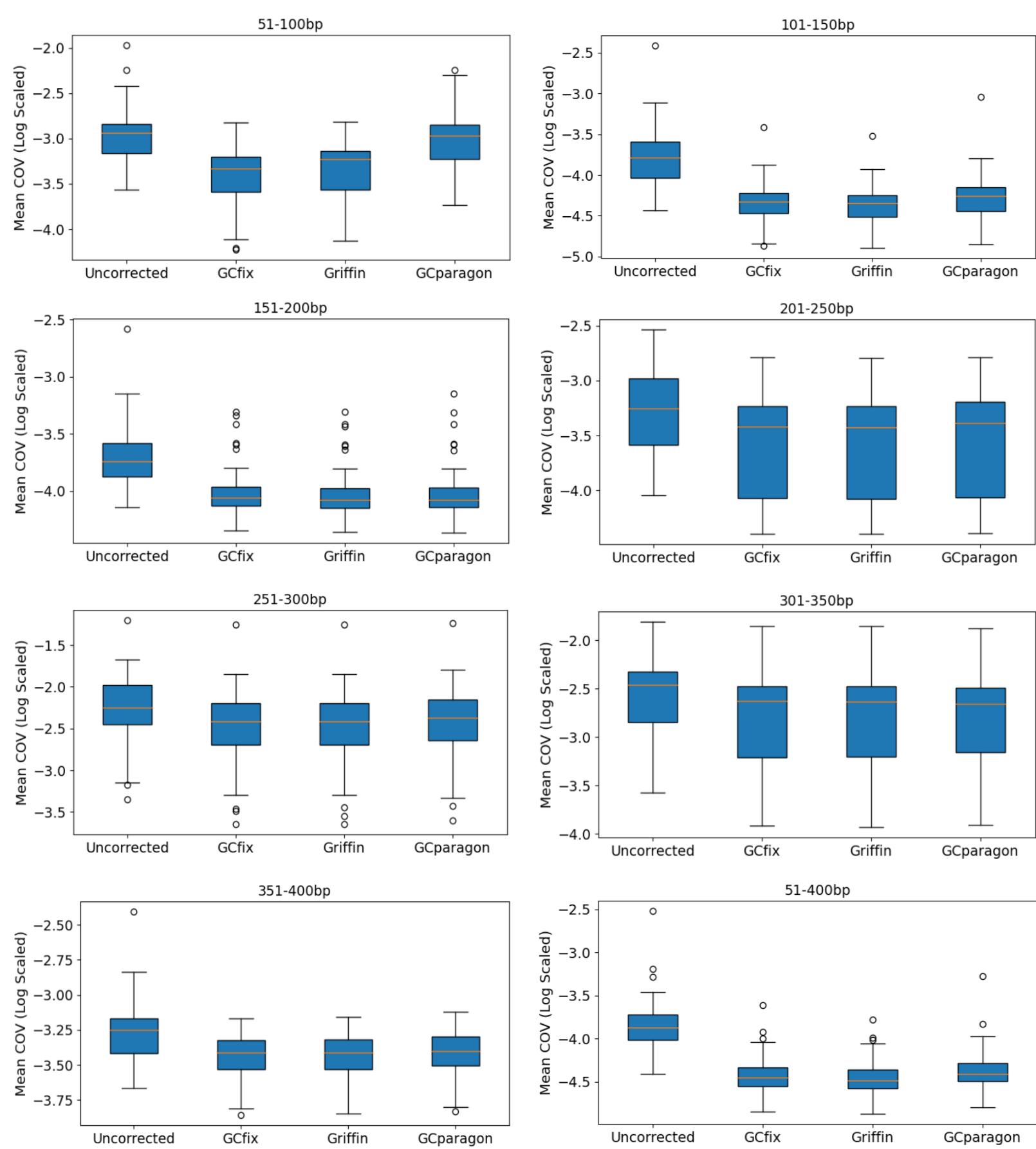
Suppl Fig S3: GC bias curves for different fragment lengths for healthy and cancer samples from different cohorts



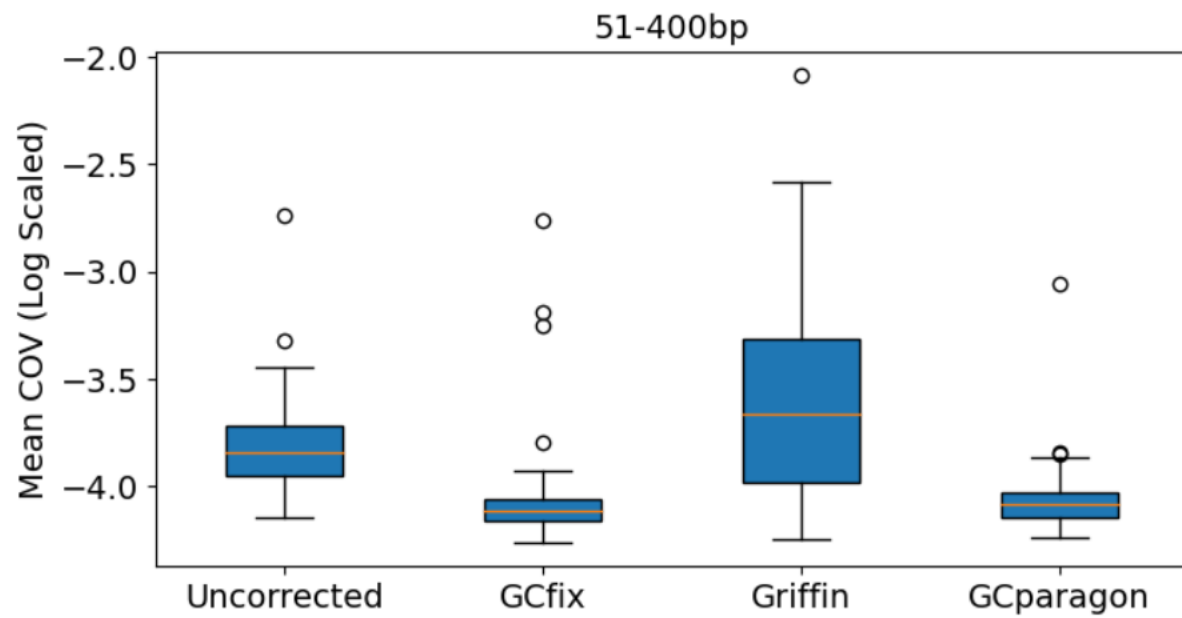
Suppl Fig S4: Sample JS divergence (log scaled) before and after correction (using different methods) from expected GC content fragment count density distribution based on different fragment length groups. **51 deep WGS (>30X)** samples (both healthy and cancer) from 4 different cohorts have been used for each box plot.



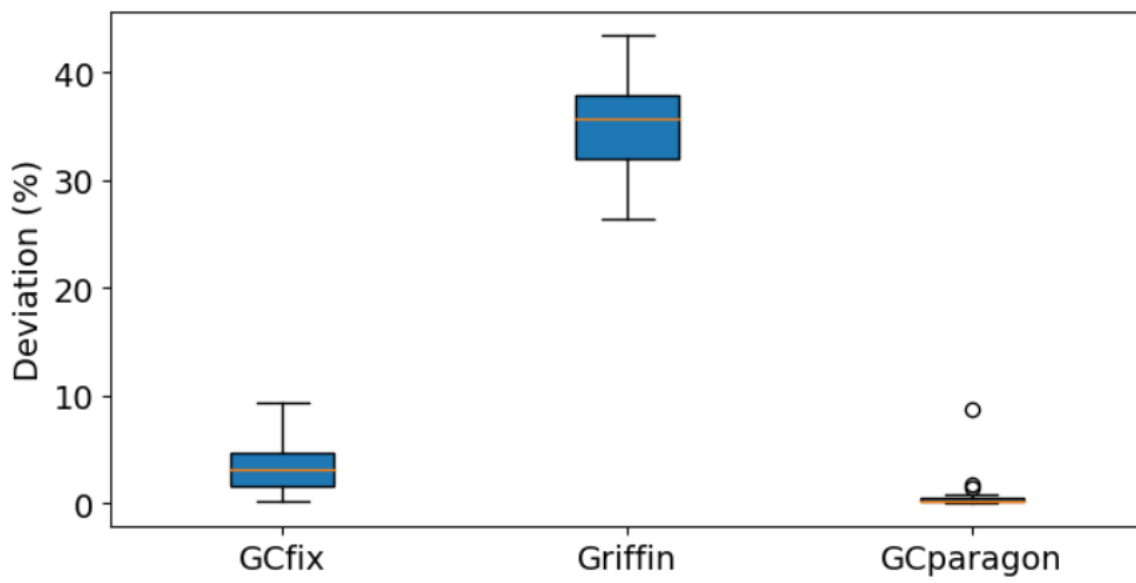
Suppl Fig S5: Sample JS divergence (log scaled) before and after correction (using different methods) from expected GC content fragment count density distribution based on different fragment length groups. 51 **ultra low pass WGS (~0.1X)** samples (both healthy and cancer) from 4 different cohorts have been used for each box plot.



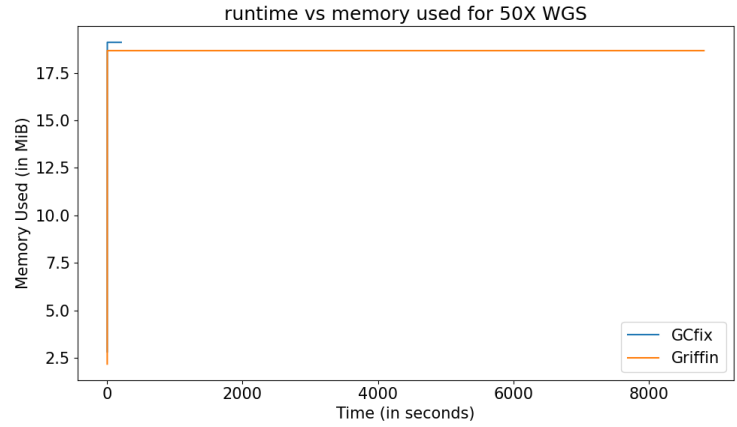
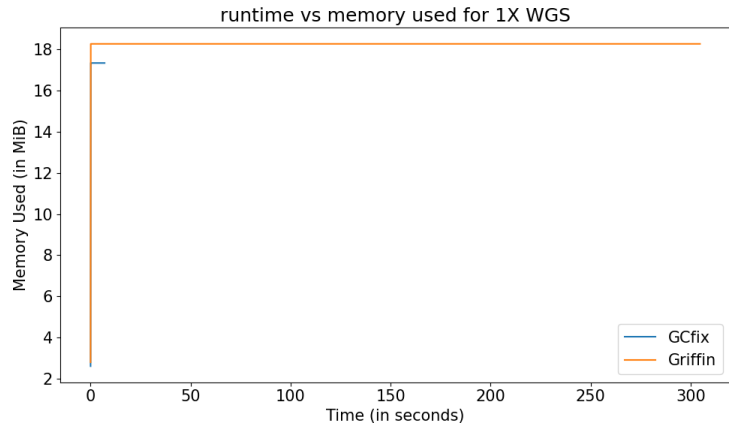
Suppl Fig S6: Sample mean coefficient of variation (log scaled) before and after correction (using different methods) based on different fragment length groups. 51 deep WGS (>30X) samples (both healthy and cancer) from 4 different cohorts have been used for each box plot.



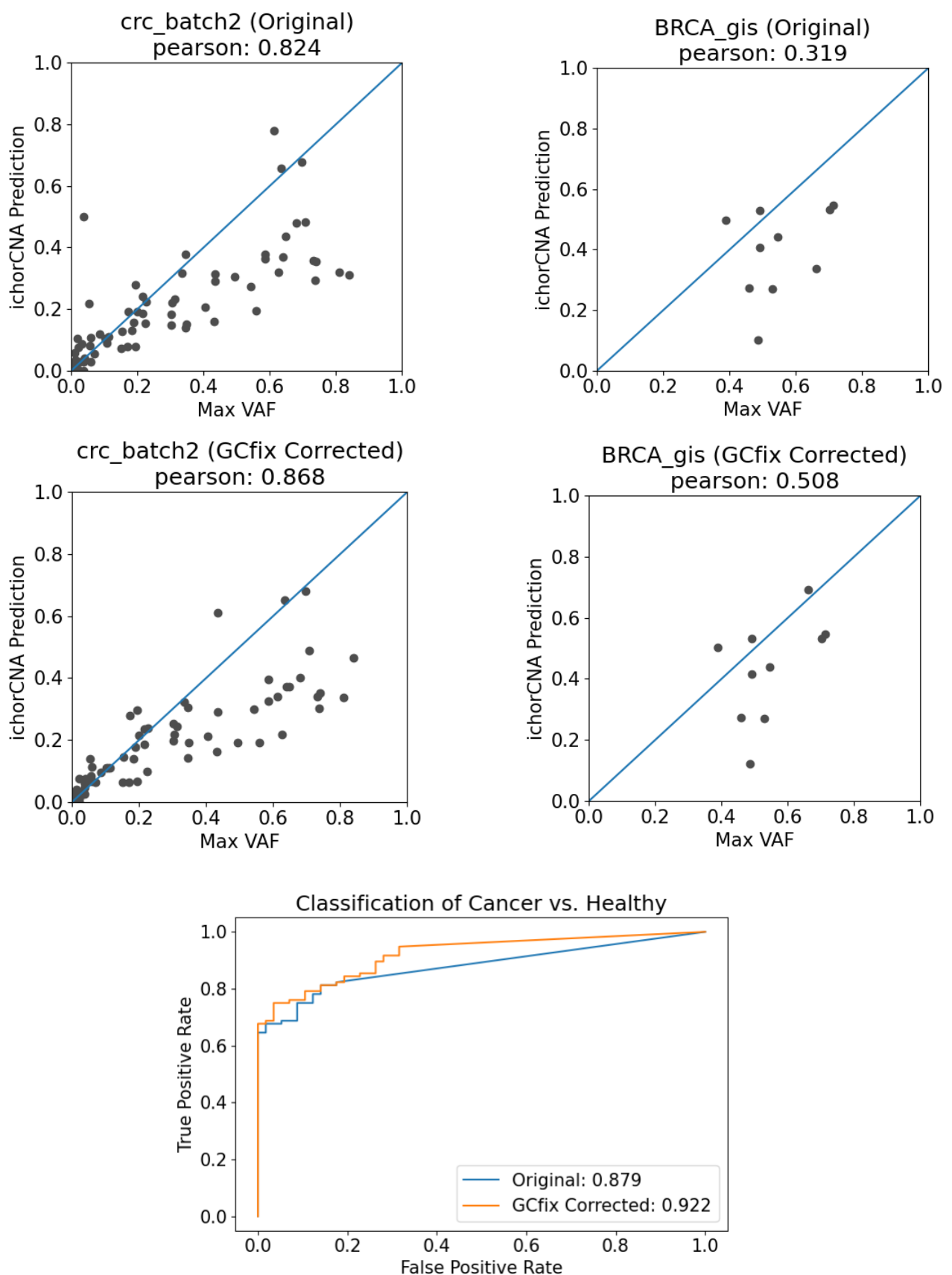
Suppl Fig S7: Sample mean coefficient of variation (log scaled) before and after correction (using different methods) based on all fragments of length 51-400bp. 51 **ultra low pass WGS (~0.1X)** samples (both healthy and cancer) from 4 different cohorts have been used for each box plot.



Suppl Fig S8: Deviation (%) in total fragment number after correction (using different methods) relative to the original uncorrected sample total fragment number using all samples (both healthy and cancer) from 4 different cohorts

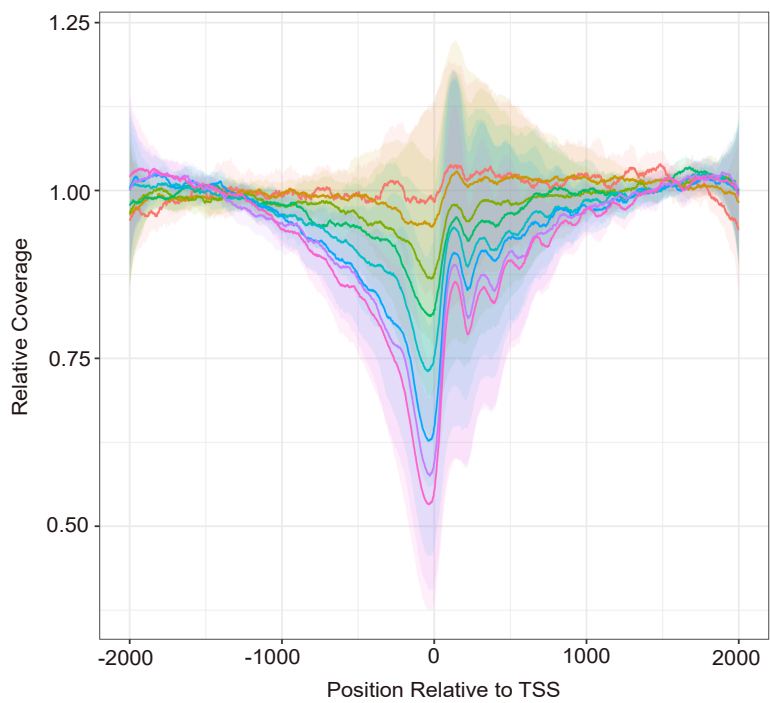


Suppl Fig S9: Runtime and memory comparison between GCfix and Griffin for 1X and 50X WGS sample

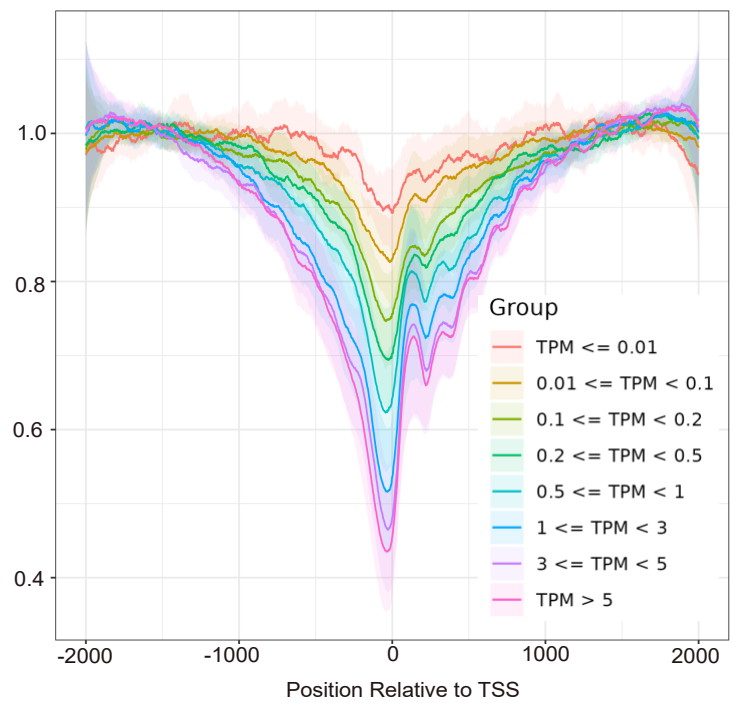


Suppl Fig S10: ichorCNA max VAF correlation and auROC plot before and after GCfix correction

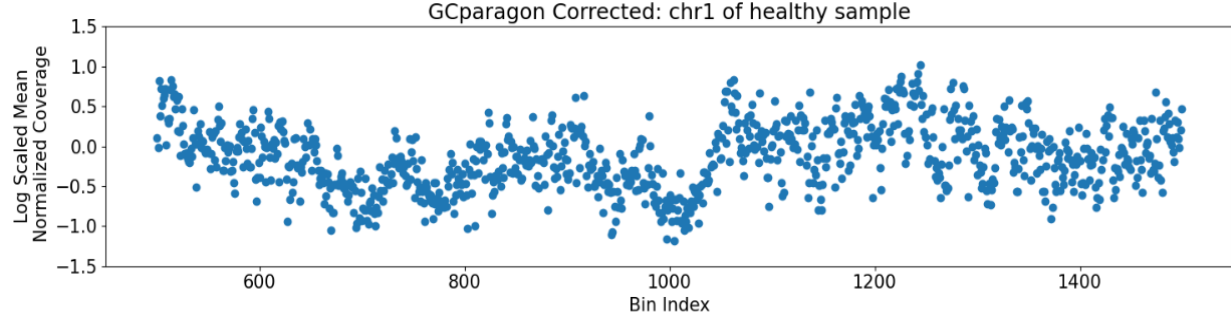
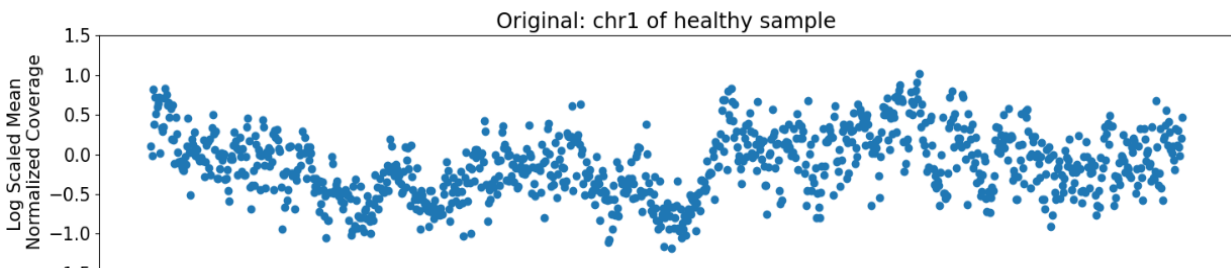
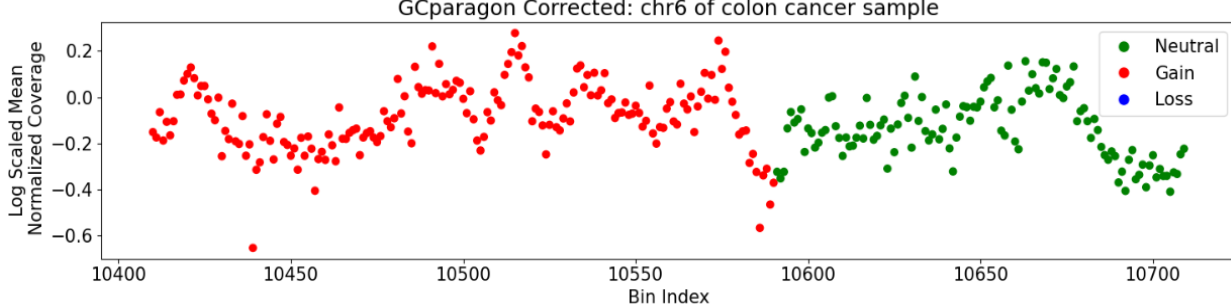
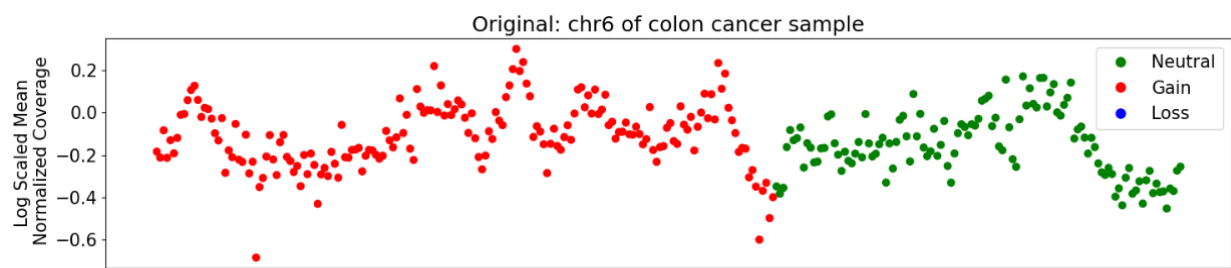
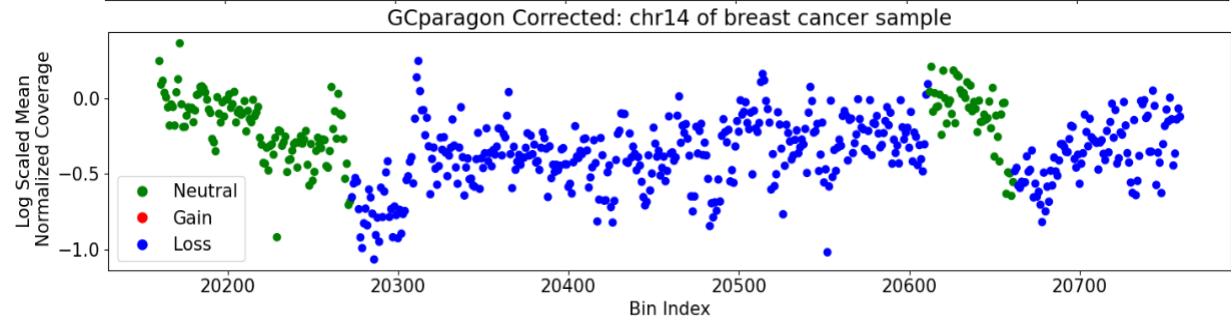
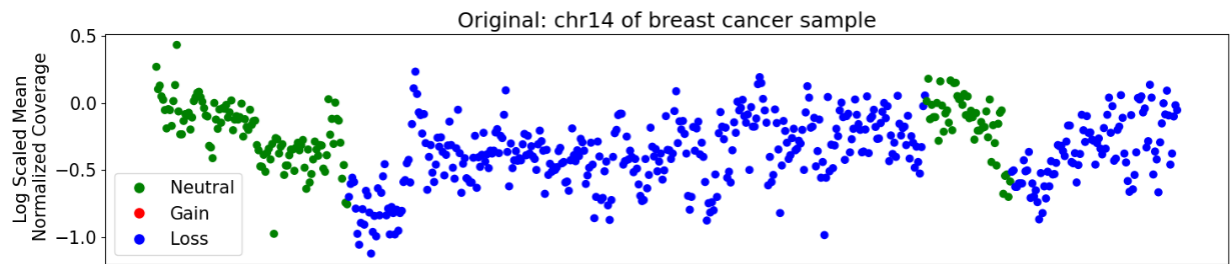
Original Uncorrected



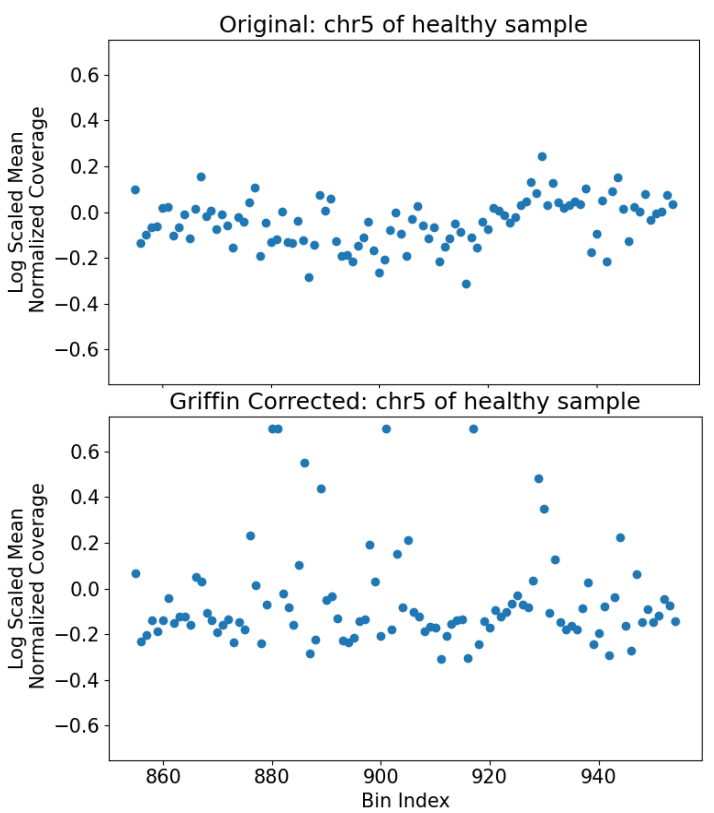
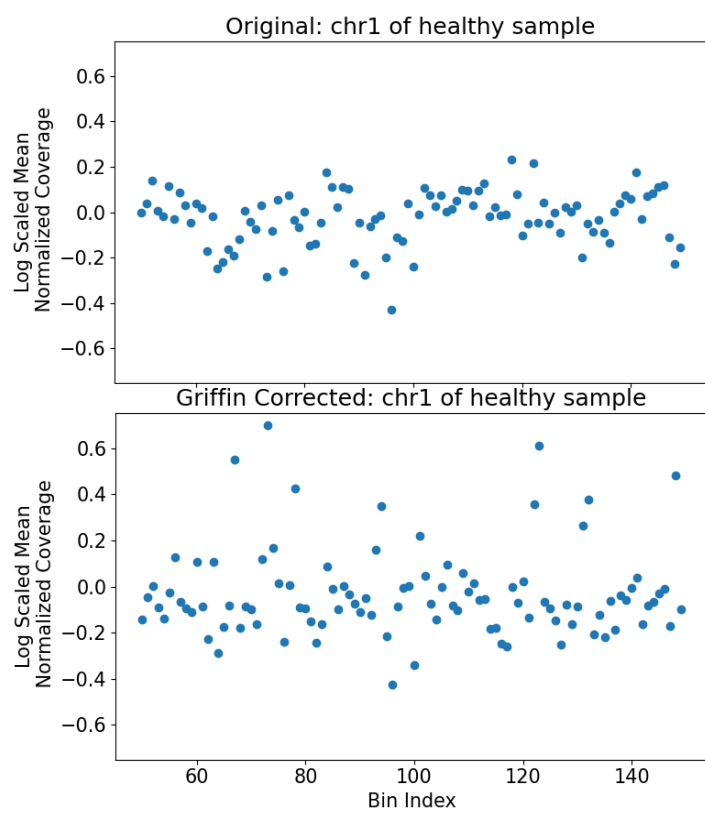
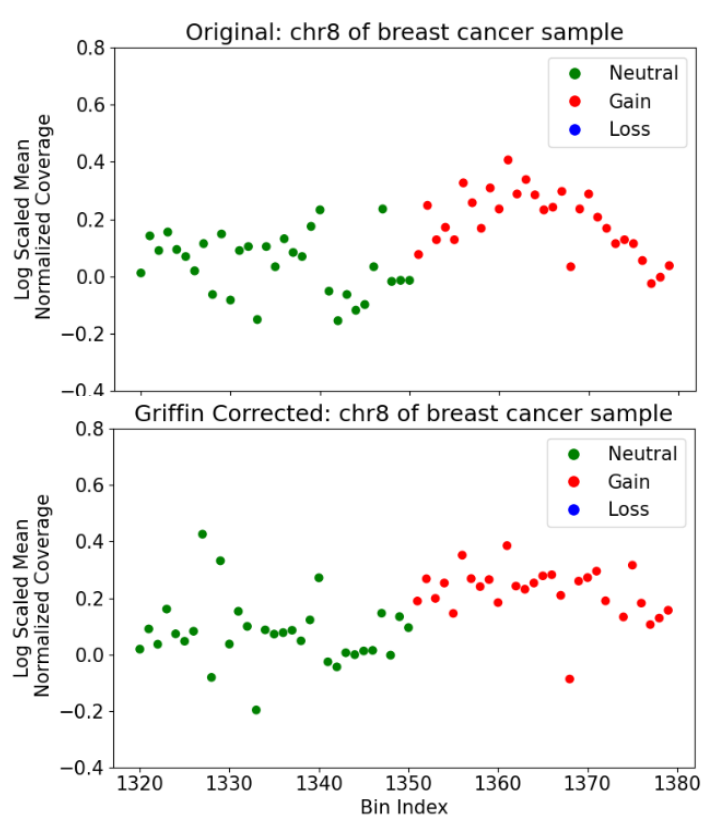
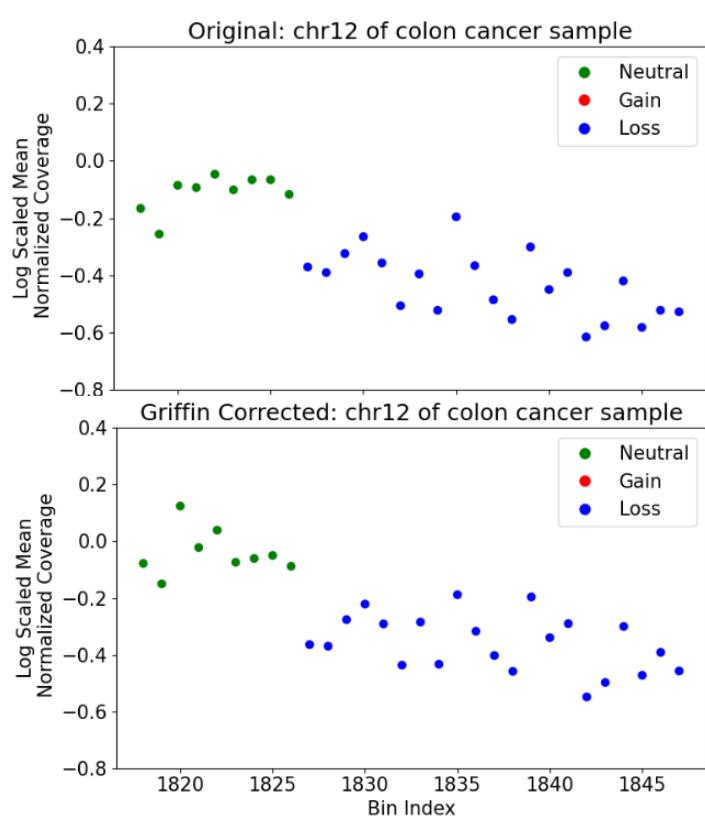
GCfix Corrected



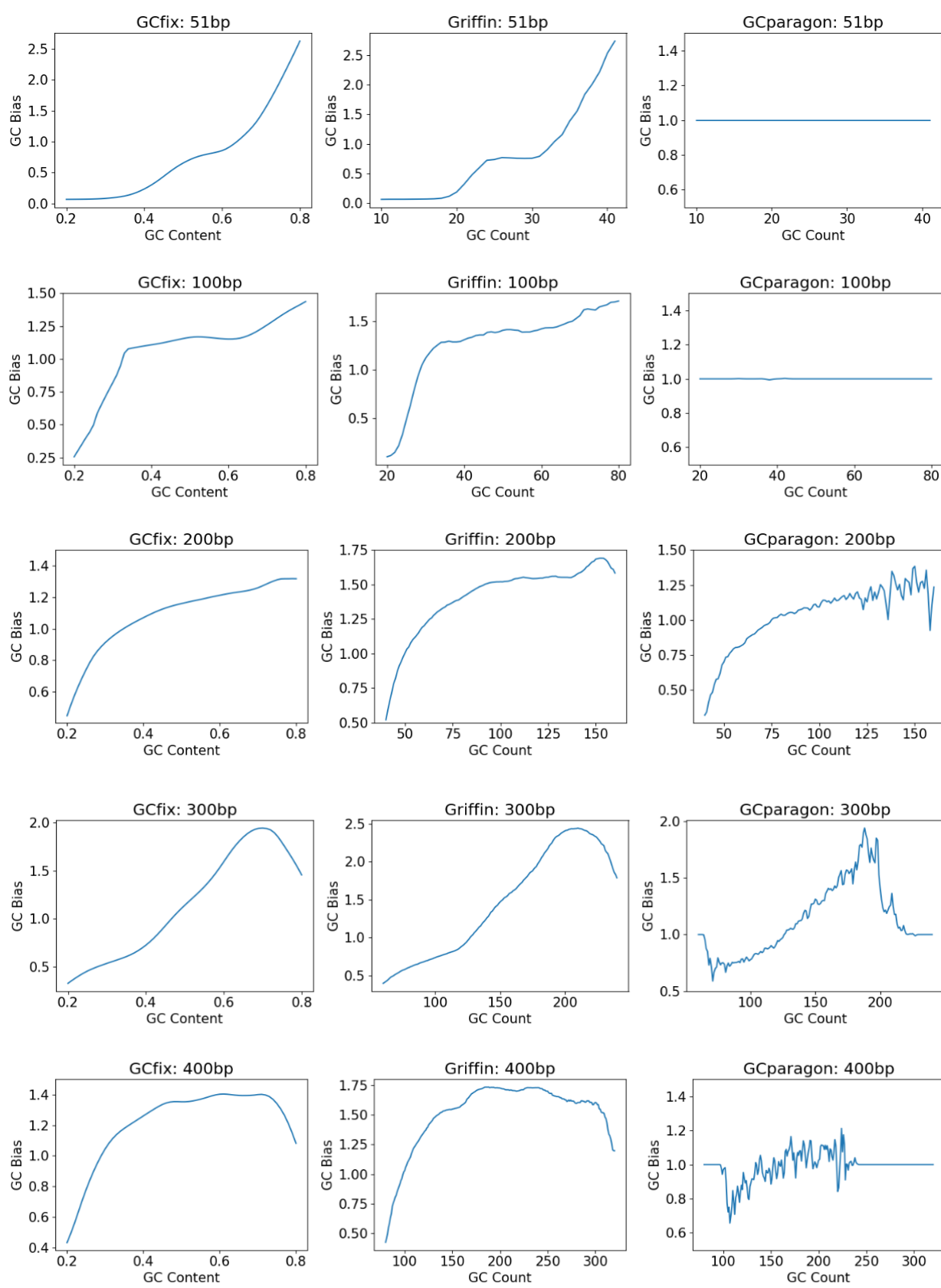
Suppl Fig S11: Relative coverage profile for different gene expression group nucleosome depleted regions (NDR) for the 17 deep WGS healthy samples before and after GCfix correction. GC correction significantly reduces the inter-sample variance in relative coverage profiles for the different gene expression groups.



Suppl Fig S12: GCparagon does not correct for short fragment (51-100bp) coverage profile for cancer and healthy samples



Suppl Fig S13: Griffin causes further disruption in the coverage profile for ultra low pass ($\sim 0.1X$) WGS cancer and healthy samples



Suppl Fig S14: Comparing GC bias curves obtained from different GC correction methods for different fragment lengths of a healthy sample